Enhanced Boundary Treatment in 2D Smoothed Particle Hydrodynamics Models

S. Marrone[1,2], M. Antuono[1], A. Colagrossi[1,3], G. Colicchio[1,3], G. Graziani[2]
[1]*INSEAN (The Italian Ship Model Basin), US3, Italy*
E-mail: s.marrone@insean.it, m.antuono@insean.it, a.colagrossi@insean.it, g.colicchio@insean.it

[2]*Department of Mechanics and Aeronautics, University of Rome "La Sapienza", Italy*
E-mail: g.graziani@uniroma1.it

[3]*CESOS: Centre of Excellence for Ship and Ocean Structures, NTNU, Trondheim, Norway*

Keywords: Lagrangian Particle Methods, SPH, solid boundary conditions, free surface flows

SUMMARY. An enhanced treatment of the solid boundaries is proposed within the two-dimensional SPH scheme. These are modeled by means of boundary particles which take the flow properties through interpolation nodes internal to the fluid. For what concerns the free surface, a fast and accurate algorithm for the free-surface detection is presented which can be easily extended to the three dimensional case.

1 INTRODUCTION

In the last years the use of particle methods to simulate complex flow has been largely increased (see e.g. [1], [2], [3]). Those methods have as a primary feature no needs of a structured topological connection (grids) between the computational nodes. In fact, these nodes are treated as fluid particles followed during their motion, while their physical properties evolve in time according to the governing equations. One of the main advantage of such methods consist in the capability in treat complex free-surface flow without an explicit enforcement of the dynamic condition along it.

Anyway, in order to analyze flows characterized by complex free surface patterns (large deformations including breaking and fragmentation of the interface) and to face a larger range of problems, it is required to know which particles belong to the free surface. The detection of the free surface, indeed, allows enforcing suitable boundary conditions along it (surface tension, isothermal condition, etc) and, consequently, dealing with different physical phenomena and flow behaviors. In the SPH literature algorithms for the free-surface tracking are already available (see for example Dilts [4] and [5]) but are generally difficult to implement and time-consuming in particular in their extension to three-dimensional simulations. In the present work a novel algorithm for the free-surface detection is presented [6]. Such a scheme, based on the properties of the SPH kernel, is easy to implement both in two and three dimensions, and computationally cheap (CPU time required is an order of magnitude lower than particle interaction calculation).

On the other hand, the enforcement of boundary conditions on solid surface is usually a drawback for the SPH schemes. In the literature several techniques have been proposed; the most used are the "repulsive-forces" [7], and the "ghost-particles" [8]. With the first one complex geometries can be easily treated though this technique does not permit to correctly evaluate local loads along the solid surface. On the other hand, the ghost-particles approach allows predicting pressure loads in a very accurate way (see e.g. [8]) but it is suitable just for plain surfaces. To overcome these drawbacks an enhanced treatment of the solid boundaries is developed by using boundary particles capable to model complex geometries and to accurately reproduce the pressure field.

2 THE SPH SCHEME

In the SPH method, the fluid domain Ω is discretized in a finite number N of *particles* representing elementary fluid volumes dV, each one with its own local mass dm and other physical properties. In this context a generic field f at the position $\boldsymbol{r}_i$ of the i-th particle is approximated through the convolution sum

$$\langle f \rangle(\boldsymbol{r}_i) = \sum_j f_j \, W(\boldsymbol{r}_i - \boldsymbol{r}_j) \, dV_j \tag{1}$$

where f_j is the value of f associated to the generic particle j, dV_j is its volume and finally $W(\boldsymbol{r}_i - \boldsymbol{r}_j)$ is a kernel function. In practical SPH computations, the choice of the kernel function affects both the CPU requirements and the stability properties of the algorithm. In this work a Gaussian kernel with a compact support has been adopted:

$$W(\boldsymbol{r}_i - \boldsymbol{r}_j) = W(r) = \begin{cases} \dfrac{1}{\pi h^2} \left[\dfrac{e^{-(r/h)^2} - C_0}{1 - C_1} \right] & \text{if } r \le \delta h \\ 0 & \text{otherwise} \end{cases} \qquad C_0 = e^{-\delta^2}, \quad C_1 = C_0 \, (1 + \delta^2)$$

where $r = \|\boldsymbol{r}_j - \boldsymbol{r}_i\|$ is the Euclidean distance between the i-th and j-th particles. The length δh represents a cut-off radius, here set equal to $3h$ as for the classical fifth-order B-spline support [9], h is called *smoothing length* and when it goes to zero the kernel function W becomes a delta Dirac function. Note that the integration of the kernel function on its support is equal to one. For the ease of notation, hereinafter we denote $W(\boldsymbol{r}_i - \boldsymbol{r}_j)$ simply through $W(\boldsymbol{r}_j)$.

The spatial derivatives of the field f can be estimated using the formula (1)

$$\langle \nabla f \rangle(\boldsymbol{r}_i) = \sum_j (\nabla f)_j \, W(\boldsymbol{r}_j) \, dV_j \tag{2}$$

After some manipulation (for more details see [10]) it is possible to move the gradient operator to the kernel and the previous formula can be approximated by

$$\langle \nabla f \rangle(\boldsymbol{r}_i) = \sum_j f_j \, \nabla_i W(\boldsymbol{r}_j) dV_j - f(\boldsymbol{r}_i) \sum_j \nabla_i W(\boldsymbol{r}_j) dV_j \tag{3}$$

where ∇_i denotes the derivative with respect to $\boldsymbol{r}_i$. One can note that this formula permits to recover exactly the null gradient of a constant function.

The largest part of the SPH schemes is built on the assumption that the fluid is barotropic and weakly-compressible. The reference equations for the flow evolution are the Euler equations:

$$\begin{cases} \dfrac{D\rho}{Dt} = -\rho \, \nabla \cdot \boldsymbol{u} \, , \\ \rho \dfrac{D\boldsymbol{u}}{Dt} = -\nabla p + \rho \, \boldsymbol{f} \\ p = c_0^2 \, (\rho - \rho_0) \, , \end{cases} \tag{4}$$

where ρ, p and $\boldsymbol{u}$ are the density, pressure and velocity fields, $\boldsymbol{f}$ is the body force field, ρ_0 is the density at the free surface and c_0 is the sound velocity. When the system (4) is written in the SPH contest, an artificial viscous term is generally added inside the momentum equation for stability

reasons (see for example [11]). In this framework, we adopt the SPH scheme proposed by Molteni & Colagrossi [12] in which a proper artificial diffusive term is used into the continuity equation in order to remove the spurious numerical high-frequency oscillations in the pressure field. Further, we add the XSPH velocity correction (see for example [11]) and an anti-clumping term similar to the one proposed by Monaghan [13]. Then, the discrete SPH scheme reads:

$$\begin{cases} \dfrac{D\rho_i}{Dt} = -\rho_i \sum_j (\boldsymbol{u}_j - \boldsymbol{u}_i) \cdot \nabla_i W(\boldsymbol{r}_j)\, \mathrm{d}V_j + \xi\, h\, c_0 \sum_j \boldsymbol{\psi}_{ij} \cdot \nabla_i W(\boldsymbol{r}_j)\, \mathrm{d}V_j\,, \\ \rho_i \dfrac{D\boldsymbol{u}_i}{Dt} = -\sum_j (p_j + p_i)\, \nabla_i W(\boldsymbol{r}_j)\, \mathrm{d}V_j \; + \; \rho_i\, \boldsymbol{f}_i \; + \; \alpha\, h\, c_0\, \rho_0 \sum_j \pi_{ij}\, \nabla_i W(\boldsymbol{r}_j)\, \mathrm{d}V_j + \\ \qquad\qquad + \chi\, h\, \dfrac{\rho_0\, c_0^2}{L} \sum_j F_{ij}\, \nabla_i W(\boldsymbol{r}_j)\, \mathrm{d}V_j\,, \\ p_i = c_0^2\, (\rho_i - \rho_0)\,, \\ \dfrac{D\boldsymbol{r}_i}{Dt} = \boldsymbol{u}_i \; + \; \epsilon \sum_j (\boldsymbol{u}_j - \boldsymbol{u}_i)\, W(\boldsymbol{r}_j)\, \mathrm{d}V_j\,, \end{cases} \tag{5}$$

where:

$$\boldsymbol{\psi}_{ij} = 2\,\left(\rho_j - \rho_i\right)\, \frac{\boldsymbol{r}_{ji}}{|\boldsymbol{r}_{ij}|^2} - \left[\, \langle \nabla\rho \rangle_i^{MLS} \; + \langle \nabla\rho \rangle_j^{MLS} \,\right], \quad \pi_{ij} = \frac{(\boldsymbol{u}_j - \boldsymbol{u}_i)\cdot \boldsymbol{r}_{ji}}{|\boldsymbol{r}_{ij}|^2}, \quad F_{ij} = \frac{h^2}{|\boldsymbol{r}_{ij}|^2}\, \exp\!\left(-8\, \frac{|\boldsymbol{r}_{ij}|^2}{h^2}\right),$$

and $\boldsymbol{r}_{ij} = -\boldsymbol{r}_{ji} = \boldsymbol{r}_i - \boldsymbol{r}_j$. The symbol $\langle \nabla\rho \rangle_i^{MLS}$ indicates that the gradient has been evaluated through a Moving Least Square interpolator (MLS hereinafter) (see [14] for more details). The symbols ρ_i, p_i and $\boldsymbol{u}_i$ denote the i-th particle density, pressure and velocity. The coefficient ξ controls the order of magnitude of the diffusive term, α the order of magnitude of the artificial viscous term and ϵ the influence of the XSPH correction on the actual velocity field. Typical values are $\alpha = 0.01$, $\epsilon = 0.25$ while ξ has been set equal to 0.1. The anti-clumping parameter χ is fixed to 0.1 while L is the characteristic length of the problem at hand. The specific choice for L is given in the section §5.

The system 5 preserves the global mass and both the linear and angular momenta. The anti-clumping term can be regarded as an internal repulsive force between fluid particles and is used to avoid the tensile instability (see [15] for more details). Finally, the diffusive term inside the continuity equation, the artificial viscosity term and the XSPH correction go to zero as the spatial resolutions increases (that is, when h goes to zero). In this way we recover the consistency with the Euler equations.

3 THE FREE SURFACE

The algorithm for the free-surface particle detection is composed of two steps: in the first one the properties of the renormalization matrix, defined by Randles and Libersky [16], are used to find particles next to the free surface. This first step strongly decreases the number of particles that will be processed in the second step. In the second step the algorithm, by means of geometric properties, detects particles that actually belong to the free surface and evaluates their local normals.

The method used to perform the first step of the algorithm was proposed by Doring [17]; it

exploits eigenvalues of the renormalization matrix defined as [16]:

$$\boldsymbol{B}(\boldsymbol{r}_i) \;=\; \Big[\; \sum_j \nabla W_j(\boldsymbol{r}_i) \otimes (\boldsymbol{r}_j \;-\; \boldsymbol{r}_i)\, dV_j \Big]^{-1} \tag{6}$$

Doring showed that if the value of the minimum eigenvalue λ of $\boldsymbol{B}$ is greater than a proper threshold, the particle does not belong to the free surface. In this way the first step of the algorithm gives a first rough detection of the free surface. This operation has a very low computational cost especially if the renormalization matrix is already computed in the SPH scheme, as *e.g.* in the formulation proposed in [16].

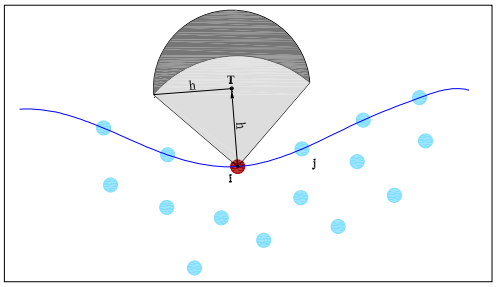

Figure 1: Sketch of the scan region used in the algorithm.

In the second step of the algorithm, a more precise and reliable control is performed on particles selected during the first step in order to complete the free surface detection. The proposed method is based on the fact that, inside the fluid domain, the sum of the kernel gradient over neighbors is very close to zero. When a particle, instead, is near the free surface, such sum is a good approximation of the local normal to the free surface (see [16]). Since the accuracy of the evaluation of this vector depends on the particle disorder, it is possible to get a more accurate evaluation by using again the renormalization matrix:

$$\boldsymbol{\nu}(\boldsymbol{r}_i) \;=\; -\boldsymbol{B}(\boldsymbol{r}_i) \sum_j \nabla W_j(\boldsymbol{r}_i)\, dV_j\,; \qquad \boldsymbol{n}(\boldsymbol{r}_i) \;=\; \frac{\boldsymbol{\nu}(\boldsymbol{r}_i)}{|\boldsymbol{\nu}(\boldsymbol{r}_i)|} \tag{7}$$

Once the vector $\boldsymbol{n}$ is known, it is possible to define a region of the domain like the one sketched in figure 1, hereinafter referred to as *scan region*. The algorithm then checks whether or not at least one neighbor particle lies in this region. If no neighbor is found inside it, the candidate particle belongs to the free surface.

4 THE SOLID BOUNDARY

In present work, an enhanced treatment of the solid boundaries is proposed within two-dimensional SPH schemes. In the specific, the solid boundary is modeled through boundary particles. Differently from the ghost particles [8], the boundary particles are fixed with respect to the solid boundary and are associated to interpolation nodes internal to the fluid through which they take the flow properties.

The algorithm to get the boundary particles is made in the following way. First, we assume the body profile to be regular and to be approximated by body nodes through the use of a spline.

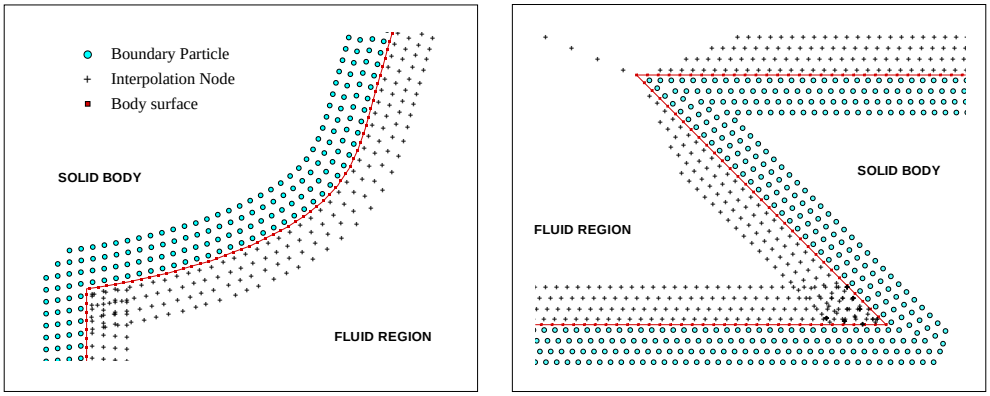

Figure 2: Sketches of boundary particles for different solid boundary profiles.

Thanks to this, we also compute the normal and the tangent unit vectors along the body profile. We assume the normal vectors to be oriented out of the fluid domain. The body nodes are equispaced with a prescribed distance ds. Then, using the normal vector, the body nodes are mirrored out of the fluid at a distance $ds/2$ from the body profile. Finally, through the use of a spline, a new profile is generated along which equispaced nodes with distance ds are set. Such a profile represents a contraction/expansion of the body profile and the nodes along it are the boundary particles. In the same way but using a vector opposite to the normal, each boundary particle is associated to an interpolation node inside the fluid. The procedure is repeated to cover the interaction radius of the fluid particles. In the specific, we build four curves of boundary particles out of the fluid and four associated curves of interpolation nodes inside the fluid (see figure 2). In case of singular points along the body profile (like corners, sharp edges etc.), the procedure described above is applied starting on each side of the singularity.

The main advantage of using the boundary particles instead of the ghost ones is that their distribution is always uniform and does not depend on the fluid particle positions. This allows a simple modeling of complex 2D geometries. Further, the use of an MLS interpolator ensures an accurate mirroring procedure of the flow quantities.

5 APPLICATIONS

In order to show the features of the proposed algorithms, we consider a dam-break problem against a sharp-edge obstacle like the one depicted in figure 3. This test case contains the most problematic configurations for the SPH schemes that is, curvilinear profiles and convex/concave angles. Along the solid boundary a free-slip condition has been imposed and nine pressure probes have been placed; six along the obstacle and three along the tank body. This test case merges together the need for a proper modeling of complex solid-boundary profiles and the necessity of an accurate description of strong flow dynamics and free-surface deformations.

In figure 4 we show some snapshots of the evolution for the dam break problem using three different spatial resolutions. The fluid motion is characterized by a violent fluid ejection caused by the sharp edge (top panels of figure 4) and by a subsequent impact on the obstacle roof (bottom panels of figure 4). Apart from the last instant ($t = 7.32\sqrt{H/g}$) which is affected by strong fragmentation of the flow and characterized by several small-spatial structures, the convergence rate is very good. This is further confirmed in the left panel of figure 5 where the convergence of the pressure field

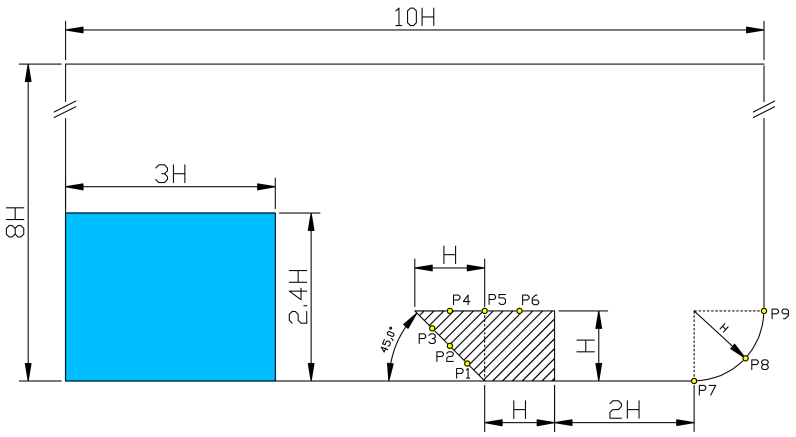

Figure 3: Sketches of the problem. Symbols P_1 to P_9 denote the pressure probes

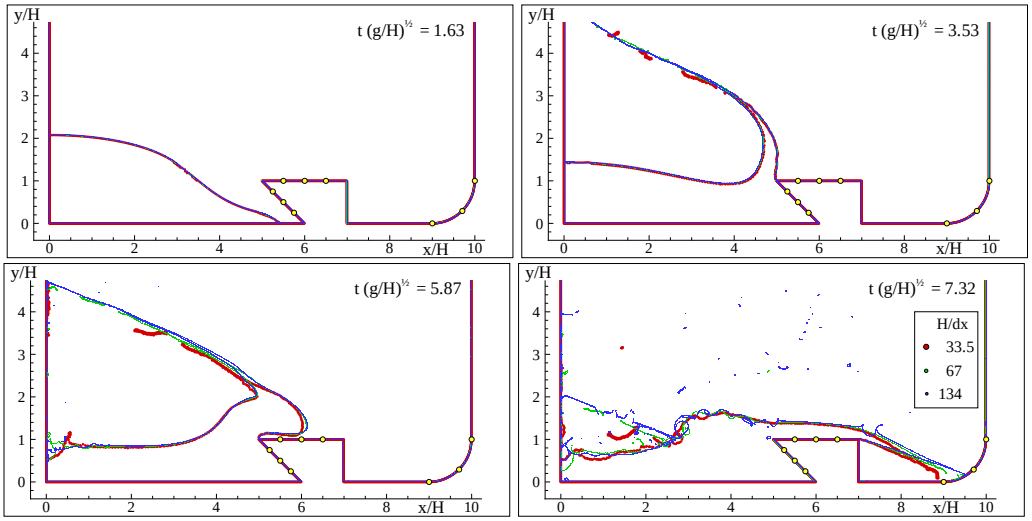

Figure 4: Convergence analysis. Red dots, $H/dx = 33.5$; green dots $H/dx = 67$; blue dots $H/dx = 234$ (dx is the mean particle distance).

evaluated at the probe P_1 (see figure 3) is shown.

On the right panel of figure 5 a detail of the velocity field near the sharp-edge is drawn just before the fluid ejection is generated. In order to check whether the weakly-compressibility assumption affects the results, in figure 6 we draw the pressure field evaluated at the probes P_1 P_1 and P_3 for two different choices of the sound velocity, c_0. As shown, the pressure signals are almost unaffected by the change in the flow compressibility.

Finally, to check the accuracy of the present model, the pressure field is compared with the one obtained through a Navier-Stokes Level-Set solver. This solver approximates the flow field with a second-order finite difference method and an approximate projection method for the solution of the Poisson equation. The free surface is modeled through a Level-Set function that delimits the water

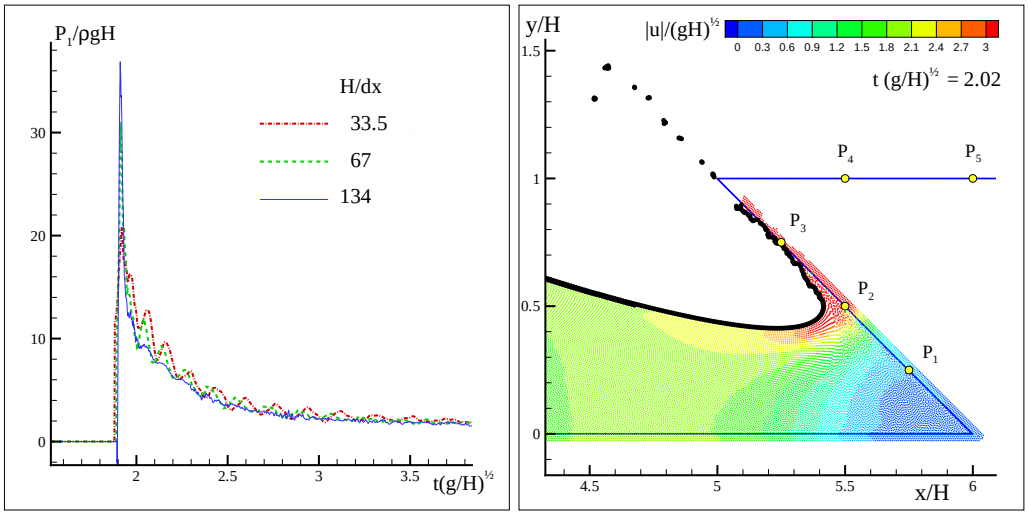

Figure 5: Left panel: convergence analysis for the pressure field evaluated at the probe P_1. Red line, $H/dx = 33.5$; green line $H/dx = 67$; blue line $H/dx = 134$ (dx is the mean particle distance). Right panel: a sketch of the velocity field at $t = 2.02\ \sqrt{H/g}$.

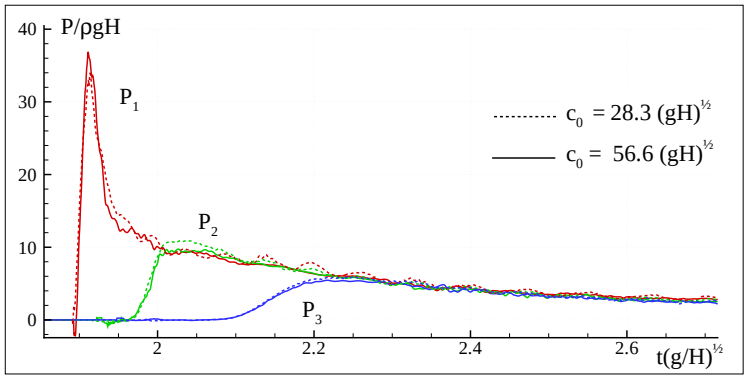

Figure 6: The pressure field evaluated at the probes P_1, P_2 and P_3 for two different values of the sound velocity ($H/dx = 134$)

field of the solution while the solid boundaries are described through a second Level-Set function that guarantees a no-slip condition as described in [18]. Since the Naveir-Stokes solver simulates the evolution of a viscous flow, we have to choose a large enough Reynolds number in order to ensure the boundary layer to be thin and to have a small influence on the global motion. In the specific we choose $Re = L\sqrt{g\,L}/\nu = 13150$ where $L = 2.4\,H$ is the initial water height.

In figure 7 we draw the comparison between the numerical solutions obtained through the SPH scheme and the Navier-Stokes Level-Set solver. The match during the first stages of the evolution is generally good. The main difference is observed in the fluid ejection that for the Navier-Stokes solver is less energetic because of the no-slip condition and because of the Level-Set function which tends to smooth the sharp profile of the fluid jet. The last instant of the evolution can be compared

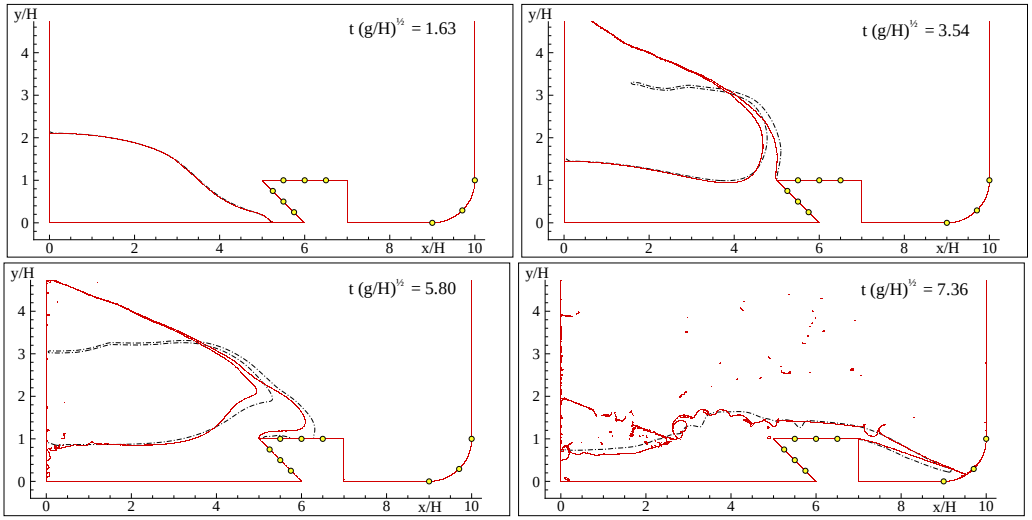

Figure 7: Comparison between the numerical solutions obtained through the SPH scheme for $H/dx = 134$ (red lines) and the Navier-Stokes Level-Set solver for $H/dx = 100$ (black lines).

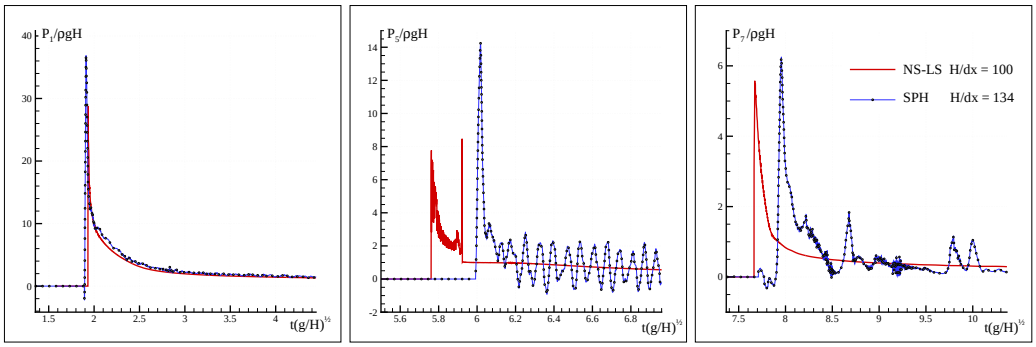

Figure 8: Comparison between the pressure field at the probe P_1, P_5 and P_7 as obtained through the SPH scheme (blue lines) for $H/dx = 134$ and the Navier-Stokes Level-Set solver (red lines) for $H/dx = 100$.

only qualitatively since the SPH solver shows an high fragmentation while the Navier-Stokes solver keeps a smoother fluid distribution.

Finally, in figure 8, we show the comparison between the pressure field as predicted by the present SPH model and the Navier-Stokes solver at the points where the fluid impacts against the solid boundary (probes P_1, P_5 and P_7). For what concerns the probe P_1, the numerical solutions match very well confirming that the early stages of the flow motion predicted by the SPH and Naveir-Stokes solvers are very similar. Conversely, for the probes P_5 and P_7 the comparison is more qualitative. This is mainly due to the different evolution of the fluid (see the bottom panels of figure 7). The pressure signal predicted by the SPH solver at the probes P_5 delays with respect to the Navier-Stokes one and shows an higher peak. Such a peak is followed by acoustic oscillations related to the weakly-compressibility assumption and generated by a cavity closure on the roof of

the obstacle. This event appears as a narrow and sharp peak in the tail of the pressure signal of the Navier-Stokes solver. Note that the cavity closure corresponds to a singularity for the Poisson equations solved by the Navier-Stokes Level-Set scheme. Finally, the right panel of figure 8 compares the pressure signals at the probe P_7. The global behavior is quite similar even though the SPH pressure signal is more noisy. This is due to the fact that the fluid jet behind the obstacle is disturbed by several drop impacts.

6 CONCLUSIONS

Novel algorithms for the treatment of the solid boundary and the free-surface detection are provided. The former allows modeling complex profiles with sharp corners and edges. The latter provides a simple and reliable method capable to follow the free-surface evolution. The algorithms have been tested by simulating a dam-break problem against a sharp-edged obstacle and validated through comparison with a Navier-Stokes Level-Set method. We believe the former test-case to be a valid benchmark for future investigations on the boundary condition implementation.

Acknowledgements

This work was partially supported by the Centre for Ships and Ocean Structures (CeSOS), NTNU, Trondheim, within the "Violent Water-Vessel Interactions and Related Structural Load" project, and partially done within the framework of the "Programma Ricerche INSEAN 2007-2009" funded by Ministero Infrastrutture e Trasporti.

References

[1] Koumoutsakos, P., "Multiscale flow simulations using particle", *Annu. Rev. Fluid Mech.*, **37**, 457–87 (2005)

[2] Landrini M., Colagrossi A., Greco M., Tulin M.P., "Gridless simulations of splashing processes and near-shore bore propagation", *Journal of Fluid Mechanics*, **591**, 183–213 (2007)

[3] Hu, X.Y., Adams, N.A., "A multi-phase SPH method for macroscopic and mesoscopic flows", *Journal of Computational Physics*, **213**, 844–861 (2006)

[4] Dilts, G.A., "Moving least-squares particle hydrodynamics II: conservation and boundaries", *Int. J. Numer. Meth. Engng* **48**, 1503-1524 (2000)

[5] Aamer, H. & Dilts, G.A., "Three-dimensional boundary detection for particle methods", *J. Comp. Phys.* **226**, 1710-1730 (2007)

[6] Marrone S., Colagrossi A., Le Touzé D., Graziani G., "A fast algorithm for free-surface particle detection in 2D and 3D SPH methods", *Proc. fourth Int. SPHeric Workshop*, Nantes, France, May 27–29, (2009)

[7] Monaghan, J.J., "Simulating free surface flows with SPH", *Journal of Computational Physics*, **110**, 399–406 (1994)

[8] Colagrossi, A., Landrini, M., "Numerical simulation of interfacial flows by Smoothed Particle Hydrodynamics", *Journal of Computational Physics*, **191**, 448–475 (2003)

[9] Monaghan J.J., "Smoothed Particle Hydrodynamics", *Ann. Rev. Astro. Astrophys.*, **30**, 543–574 (1992)

[10] Colagrossi A., Antuono M., Le Touzé D., “Theoretical considerations on the free surface role in the SPH model”, *Phys. Rev. E.*, 79/5: 056701:1–13 (2009)

[11] Monaghan J.J.,“Smoothed Particle Hydrodynamics”, *Rep. Prog. Phys.*, **68**: 1703–1759 (2005)

[12] Molteni D. & Colagrossi A., “A simple procedure to improve the pressure evaluation in hydrodynamic context using the SPH”, *Computer Physics Communications*, In Press, Corrected Proof available online, (2008)

[13] Monaghan, J.J., “SPH without a Tensile Instability”, *Journal of Computational Physics*, **159**, 290–311 (2000)

[14] Fries T.P.& Matthies H.G., “Classification and Overview of Meshfree Methods”, *Informatikbericht 2003-03, Institute of Scientific Computing*, Technical University Braunschweig, Brunswick, Germany, (2004)

[15] Swegle J.W., Hick D.L., Attaway S.W., “Smoothed Particle Hydrodynamics Stability Analysis”, *Journal of Computational Physics*, **116**, 123–134 (1995)

[16] Randles, P.W. & Libersky, L.D., “Smoothed Particle Hydrodynamics: Some recent improvements and applications”, *Comput. Methods Appl. Mech. Engng.*, **139**, 375-408 (1996)

[17] Doring, M., “Développement d’une méthode SPH pour les applications à surface libre en hydrodynamique”, *PhD Thesis, Ecole Centrale Nantes* (2005)

[18] Colicchio G., “Violent disturbance and fragmentation of free surfaces”, *PhD Thesis, University of Southampton* (2004)